Supplemental Material
Two-Body Contact Dynamics in a Bose Gas near a Fano-Feshbach Resonance

Alexandre Journeaux,[1] Julie Veschambre,[1] Maxime Lecomte,[1] Ethan Uzan,[1]
Jean Dalibard,[1] Félix Werner,[1] Dmitry S. Petrov,[2] and Raphael Lopes[1,*]

[1]*Laboratoire Kastler Brossel, Collège de France, CNRS, ENS-Université PSL, Sorbonne Université, 11 Place Marcelin Berthelot, 75005 Paris, France*
[2]*Université Paris-Saclay, CNRS, LPTMS, 91405, Orsay, France*

Density-dependence of losses

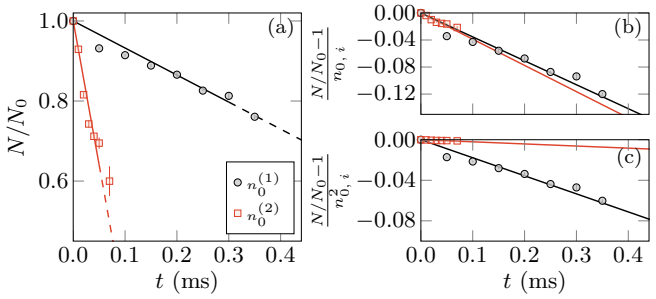

FIG. S1. Loss rate as a function of density. (a) Atom number evolution as a function of time t for two different initial densities (see legend and text), following a quench to the FFR. At short times, losses exhibit a linear dependence on time. (b) Atom number normalized by the initial peak density. The data collapse onto a single linear curve, consistent with a two-body loss process. (c) Atom number normalized by the square of the initial peak density. The differing evolutions clearly indicate that the losses are incompatible with a three-body process.

In this section, we describe the procedure that leads to the conclusion that the losses in our experiment have a two-body nature. The differential equation

$$\dot{n} = -\mathcal{L}_\alpha n^\alpha \tag{S1}$$

describes the evolution of the density in the presence of a loss mechanism involving α-body collisions. In our experiment, the single-particle lifetime is on the order of 15 s, far exceeding the timescales probed here. The dominant loss mechanisms are therefore either dimer losses involving photon-assisted photodissociation ($\alpha = 2$) or intrinsic three-body losses ($\alpha = 3$). Assuming a Gaussian spatial distribution, and integrating over space, the total atom number then evolves according to:

$$\dot{N} = -\frac{\mathcal{L}_\alpha n_0^{\alpha-1}}{\alpha^{3/2}} N\,. \tag{S2}$$

Its solution, neglecting the time-dependence of $\mathcal{L}_\alpha$, is given by

$$N(t) = \frac{N_0}{\left[1 + \left(\frac{\alpha-1}{\alpha^{3/2}}\right)\mathcal{L}_\alpha n_{0,i}^{\alpha-1} t\right]^{1/(\alpha-1)}} \tag{S3}$$

where $n_{0,i} = N_0/V$ is the peak density at $t = 0$, N_0 the initial atom number and $V = \left[2\pi k_B T/\left(m\bar{\omega}^2\right)\right]^{3/2}$ the volume. We restrict to short enough times such that the temperature of the cloud changes by less than 15% of its initial value. For these short times, Eq. (S3) simplifies to

$$\frac{N(t)}{N_0} \approx 1 - \mathcal{L}_\alpha \frac{n_{0,i}^{\alpha-1}}{\alpha^{3/2}} t\,. \tag{S4}$$

We investigate two thermal samples at the same temperature, $T = 0.9\,\mu\text{K}$, but with different geometric mean trap frequencies: $\bar{\omega}^{(1)} = 2\pi \times 141\,\text{Hz}$ and $\bar{\omega}^{(2)} = 2\pi \times 212\,\text{Hz}$. The initial atom numbers are such that $N_0^{(2)} \approx 3\,N_0^{(1)}$, and therefore $n_{0,i}^{(2)} \approx 10\,n_{0,i}^{(1)}$.

In Fig. S1(a), we show the evolution of $N(t)/N_0$ as a function of t, confirming the initial linear decrease in atom number for both cases. We then examine the power-law dependence of the loss rate on the density. From Eq. (S4) we expect that the quantity $[N(t)/N_0 - 1]/n_{0,i}^{\alpha-1} \approx -(\mathcal{L}_\alpha/\alpha^{3/2})\,t$ is independent of $n_{0,i}$. We find that the experimentally measured values for this quantity do indeed approximately collapse on a single curve if we assume $\alpha = 2$ (Fig. S1b), but not for $\alpha = 3$ (Fig. S1c). We conclude that the losses are predominantly two-body in nature. We performed the same analysis for different temperatures and densities, and reached the same conclusion.

To theoretically explain why three-body losses are negligible in our regime, one would need to solve the three-body problem for lossy and narrow two-body resonances (e.g., by generalizing the method developed in Ref. [1]), which is beyond the scope of this work. We can nevertheless provide a simple order-of-magnitude estimate in the large-$R^\star$ limit, where the relaxation rate of bare closed-channel molecules colliding with free atoms, Γ_{3B}, is on the order of $\hbar\ell_{vdW}n/m$. For the typical densities used in this work, this yields $\Gamma_{3B} \approx 0.016\,\text{ms}^{-1}$, which is more than 4 orders of magnitude smaller than the photo-dissociation loss rate $\Gamma_b^{on} \approx 754\,\text{ms}^{-1}$ from Eq. (7).

Cycling procedure

As described in the main text, we quench the system to resonance for a duration t_{on}, followed by an off-resonant period t_{off}. The total exposure time at resonance is given by $t_{exp} = N_{cycles}\,t_{on}$. We use integer values of N_{cycles}, corresponding to square pulses generated by a waveform generator that

modulates the radiofrequency amplitude driving an acousto-optic modulator. Although $t_{\rm exp}$ takes discrete values, the variation of N over one cycle is small, and N can be considered to be a smooth differentiable function of $t_{\rm exp}$. In practice, the maximum number of cycles ranges from 10 to 5000 depending on the chosen value for $t_{\rm on}$.

Extracting L_2 in a Thermal Gas with Evolving Temperature

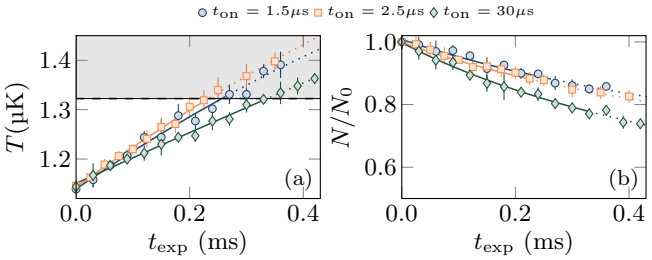

FIG. S2. Temperature and atom number evolution. (a) Temperature evolution as a function of time after quenching a thermal sample with initial temperature $T = 1.15\,\mu$K to the Fano–Feshbach resonance, for different interrogation times $t_{\rm on}$ (see legend) and $t_{\rm off} = 26\,\mu$s. The shaded area corresponds to a temperature increase greater than 15% of the initial temperature, where we exclude all data from our analysis. The lines are fits to the data using a polynomial function. (b) Normalized atom number evolution as a function of time. The fitted curves correspond to the resolution of Eq. (S5) accounting for the temperature evolution extracted from the fits shown in (a).

Atom loss is accompanied by heating in the harmonic trap, as shown in Fig. S2(a), resulting in a variation of the effective volume due to the thermal expansion of the cloud. To ensure accurate determination of the two-body loss rate, we restrict our analysis to the regime where the temperature increases by no more than 15%, as indicated by the shaded area in Fig. S2(a).

Equation (1) of the main text yields the differential equation

$$\frac{dN}{dt_{\rm exp}} = -L_2(\bar{T})\,N(t_{\rm exp})^2 \Big/ \left[\frac{4\pi k_B}{m\bar{\omega}^2}\,T(t_{\rm exp})\right]^{3/2}, \qquad \text{(S5)}$$

which we solve numerically, with $T(t_{\rm exp})$ obtained by fitting the measured temperature evolution with a second order polynomial (see Fig. S2). This allows us to account for the dilatation of the sample over time. We use the fitted temperature curve to determine the time-average temperature $\bar{T}$ which is used in the computation of the corresponding two-body loss rate.

Temperature dependence of the loss resonance feature

A consequence of the narrowness of the FFR is that for nonzero temperature, the maximum loss rate does not occur exactly when the scattering length diverges. For a fixed trap frequency, we show in Fig. S3 that the magnetic field at which losses are maximal, $B_{\rm max}$, indeed shifts with temperature. We

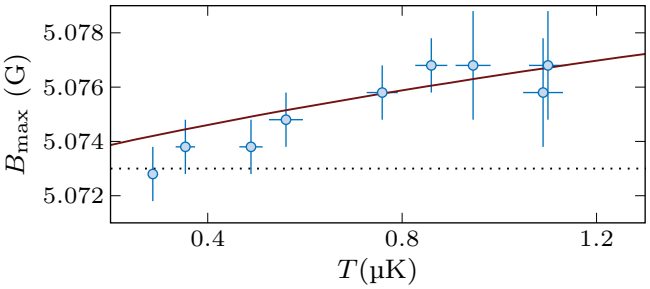

FIG. S3. Magnetic field $B_{\rm max}$ at which the loss rate is maximal, shown versus the sample temperature. The trap frequencies are fixed at $(\omega_x, \omega_y, \omega_z) = 2\pi \times (58, 358, 292)$ Hz for all data. The dotted line indicates the FFR position obtained from closed-channel molecular spectroscopy. The solid line is the theoretical prediction for $B_{\rm max}$ which maximizes Eq. (5) of the main text.

note for completeness that $t_{\rm exp}$ was adjusted at each temperature such that the maximum loss corresponds to 30% of the initial atom number.

The experimentally determined $B_{\rm max}$ is in good agreement with the theoretical prediction (see solid line in Fig. S3) obtained from Eq. (5) without adjustable parameters (we use $R^\star$ and $\Gamma_{\rm b}^{\rm on}$ from Eq. (7), and $\delta\mu$ and $B_{\rm res}$ from Tab. I, right column).

Fitting procedure to extract $R^\star$ and $\Gamma_{\rm b}^{\rm on}$

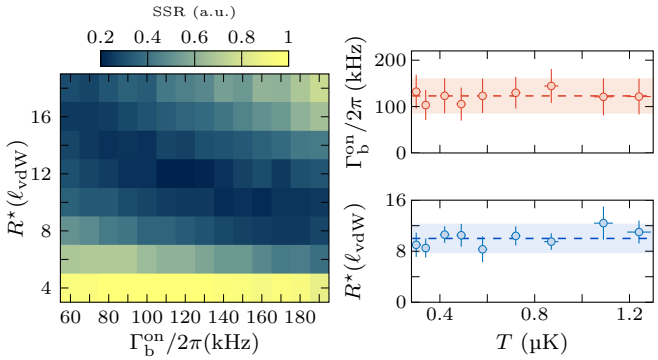

FIG. S4. Temperature-dependence of fitted parameters. Left panel: Sum of squared residuals (SSR) for the data at $T = 1.09(4)\,\mu$K. Right panels: $\Gamma_{\rm b}^{\rm on}$ and $R^\star$ *vs.* temperature. Here dashed lines indicate temperature averages and shaded regions show the associated standard deviations.

To compare the experimental data with the numerical simulations for $L_2(t_{\rm on}, t_{\rm off})$, we use a Floquet-based numerical approach that solves Eq. (4) with periodic $E_0(t)$ and averages the instantaneous loss rate over a full modulation cycle, $t_{\rm on}+t_{\rm off}$ (see Ref. [2] and the last section of this Supplemental Material), which depends on both on- and off-resonant parameters.

For the off-resonant scattering length we use $a'_{\rm off} \approx 46\,a_0$ (see End Matter). For the on-resonant scattering length $a'_{\rm on}$, we

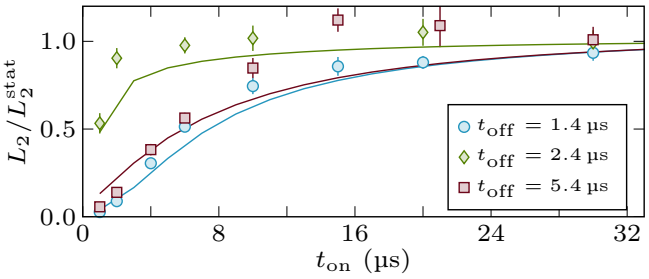

FIG. S5. Evolution of L_2 as a function of $t_{\rm off}$ and $t_{\rm on}$. Buildup of the two-body loss rate $L_2(t_{\rm on})$ for various out-of-resonance duration $t_{\rm off}$ (see legend) at a fixed temperature of $T = 0.41\,\mu$K. Solid lines are numerical solutions of Eq. (4) using $\Gamma_{\rm b}/2\pi = 123\,$kHz and $\mathrm{Re}(E_0)/h = -560\,$kHz.

use the value that maximizes Eq. (5) of the main text for each temperature (see previous section). Regarding the molecular decay rate $\Gamma_{\rm b}(t)$, we assume that $\Gamma_{\rm b}(t) = \Gamma_{\rm b}^{\rm on}$ during the on-resonant interval $t_{\rm on}$ and $\Gamma_{\rm b}(t) = \Gamma_{\rm b}^{\rm off}$ during the off-resonant time $t_{\rm off}$. For each temperature, we fit the data by minimizing the sum of the squared residuals with respect to the numerical simulation, while varying $R^\star$, $\Gamma_{\rm b}^{\rm on}$, and $\Gamma_{\rm b}^{\rm off}$. We observed that $\Gamma_{\rm b}^{\rm off}$ had little impact on the fits, and therefore fixed it to the value $2\pi \times 20\,$kHz obtained by modulation spectroscopy (see Tab. I).

The fitting procedure thus reduces to a two-dimensional optimization over $R^\star$ and $\Gamma_{\rm b}^{\rm on}$. Specifically, we vary $R^\star$ in the range $4\,\ell_{\rm vdW}$ to $18\,\ell_{\rm vdW}$, and $\Gamma_{\rm b}^{\rm on}$ from 60 kHz to 190 kHz. For all temperatures, we observe a well-defined optimal region in parameter space (see Fig. S4, left panel). The error bars on the fitted parameters are obtained using a bootstrap method. In the right panels of Fig. S4, we check the temperature independence of $R^\star$ and $\Gamma_{\rm b}^{\rm on}$, respectively. The dashed lines and shaded areas represent the temperature-averaged values and their standard deviations, yielding $R^\star = 10.0(2.3)\,\ell_{\rm vdW}$ and $\Gamma_{\rm b}^{\rm on}/2\pi = 123(38)\,$kHz.

Evolution of L_2 as a function of $t_{\rm on}$ and $t_{\rm off}$

We show in Fig. S5 the buildup of the two-body loss rate, normalized by its asymptotic value $L_2^{\rm stat} = 283(19)\,\mu\mathrm{m}^3/\mathrm{s}$, as a function of $t_{\rm on}$ for three different values of $t_{\rm off}$ (see legend). Although the overall behavior of L_2 is non-monotonic with respect to $t_{\rm off}$ (see Fig. 4 and its discussion in the main text), we observe a monotonic increase of L_2 with $t_{\rm on}$ for each individual $t_{\rm off}$. Importantly, we find that for a fixed modulation period, i.e., the same value of $t_{\rm on} + t_{\rm off}$, the measured two-body loss rate can vary significantly. For example, for $t_{\rm off} = 1.4\,\mu$s and $t_{\rm on} = 2\,\mu$s, we find $L_2/L_2^{\rm stat} = 0.089(7)$, whereas for the same total modulation period but with $t_{\rm off} = 2.4\,\mu$s and $t_{\rm on} = 1\,\mu$s, we measure $L_2/L_2^{\rm stat} = 0.53(6)$.

Derivation of the evolution equations for the closed-channel amplitude

We solve the problem of two atoms in a large volume, which can be taken to be a unit volume to alleviate notations. This is equivalent to the second order non-equilibrium virial expansion of Refs. [3–5]. Although we deal with identical bosons, for future reference we provide the derivation of the evolution equations for two distinguishable atoms of generally different masses. Consider the two-channel Hamiltonian (we set $\hbar = 1$)

$$\hat{H} = \int d^3r \sum_{\sigma=1,2} \hat{\psi}_\sigma^\dagger(\mathbf{r}) \left(-\frac{\nabla_{\mathbf{r}}^2}{2m_\sigma}\right) \hat{\psi}_\sigma(\mathbf{r}) + \hat{\psi}_b^\dagger(\mathbf{r}) \left[-\frac{\nabla_{\mathbf{r}}^2}{2(m_1+m_2)} + \nu(t)\right] \hat{\psi}_b(\mathbf{r})$$
$$- \eta \int d^3r\, d^3y\, \delta_{r_0}(\mathbf{y}) \left[\hat{\psi}_1^\dagger(\mathbf{r} + \mu\mathbf{y}/m_1)\, \hat{\psi}_2^\dagger(\mathbf{r} - \mu\mathbf{y}/m_2)\, \hat{\psi}_b(\mathbf{r}) + h.c.\right], \tag{S6}$$

where $\hat{\psi}_1^\dagger(\mathbf{r})$ and $\hat{\psi}_2^\dagger(\mathbf{r})$ create atoms of masses m_1 and m_2, respectively, $\hat{\psi}_b^\dagger(\mathbf{r})$ is the creation operator of a bare closed-channel molecule, and $\mu = m_1 m_2/(m_1+m_2)$ is the effective mass. To regularize the model we use the delta-shell representation with $\delta_{r_0}(\mathbf{y}) = \delta(|\mathbf{y}| - r_0)/(4\pi r_0^2)$, were r_0 is assumed to be the smallest length scale in the problem. As we will see, the model (S6) has a well-defined zero-range limit such that r_0 drops out of the final equations and the bare parameters ν (complex) and η (real) are expressed in terms of the renormalized physically meaningful quantities: the complex detuning $E_0(t) = \mathrm{Re}\,[E_0(t)] - i\,\Gamma_{\rm b}(t)/2$ and the real range parameter $R^\star$ characterizing the resonance width (a standard procedure also used, e.g., in Refs. [6, 7]). We note that it is possible to add a direct interaction between atoms in the open channel, characterized in the zero-range limit by the background scattering length (see, e.g., Refs. [5, 8, 9]); we have checked that for our experimental parameter regime, this does not lead to any significant changes of the results, and we omit the background interaction to simplify the discussion.

The center-of-mass degree of freedom separates and the

relative two-body wave function can in general be written as

$$\int d^3r\, d^3y\, \Psi(\mathbf{y},t)\, \hat{\psi}_1^\dagger(\mathbf{r}+\mu\mathbf{y}/m_1)\, \hat{\psi}_2^\dagger(\mathbf{r}-\mu\mathbf{y}/m_2)\, |0\rangle + \int d^3r\, \phi(t)\, \hat{\psi}_b^\dagger(\mathbf{r})\, |0\rangle\,, \quad \text{(S7)}$$

where $|0\rangle$ is the vacuum state. The evolution of the amplitudes Ψ and ϕ is governed by the coupled Schrödinger equations

$$i\partial_t \Psi(\mathbf{y},t) = -\frac{\nabla_\mathbf{y}^2}{2\mu}\Psi(\mathbf{y},t) - \eta\,\delta_{r_0}(\mathbf{y})\,\phi(t) \quad \text{(S8)}$$

and

$$i\partial_t \phi(t) = \nu(t)\,\phi(t) - \eta\int d^3y\,\delta_{r_0}(\mathbf{y})\,\Psi(\mathbf{y},t). \quad \text{(S9)}$$

Equation (S8) describes free motion everywhere in space except for the surface of the sphere with radius r_0. It is useful to rewrite this equation in the integral form

$$\Psi(\mathbf{y},t) = \Psi_0(\mathbf{y},t) + i\,\eta\int_{-\infty}^{t} dt' \int d^3y'\, G(\mathbf{y}-\mathbf{y}',t-t')\,\delta_{r_0}(\mathbf{y}')\,\phi(t'), \quad \text{(S10)}$$

where the Green function

$$G(\mathbf{y},t) = \frac{e^{iy^2\mu/2t}}{(2\pi i t/\mu)^{3/2}} \quad \text{(S11)}$$

solves

$$[i\partial_t + \nabla_\mathbf{y}^2/(2\mu)]G(y,t) = i\,\delta(t)\,\delta(\mathbf{y}) \quad \text{(S12)}$$

and $\Psi_0(\mathbf{y},t)$ is a solution of Eq. (S8) with η set to zero. For our scattering problem this is the incoming plane wave $\Psi_0(\mathbf{y},t) = e^{i\mathbf{k}\cdot\mathbf{y}-ik^2t/(2\mu)}$ with momentum $\mathbf{k}$.

The idea of passing from Eq. (S8) to Eq. (S10) is that, if we now set $|\mathbf{y}| = r_0$, Eqs. (S9) and (S10) form a closed system of equations for $\phi(t)$ and $\Psi(\mathbf{y},t)$, where $\mathbf{y}$ is on the sphere. Moreover, Eq. (S10) [as well as the original Hamiltonian (S6)] conserves angular momentum and allows for a separate description of each partial wave. In our case the s-wave scattering is dominant and for brevity we concentrate on this channel, which means that we deal with two time-dependent functions $\phi(t)$ and $\Psi(r_0,t)$. Working out the integral over d^3y in the limit of small r_0 Eq. (S10) reduces to

$$\Psi(r_0,t) = e^{-ik^2t/(2\mu)} + \frac{\eta\phi(t)}{2\pi r_0/\mu} + i\eta\int_{-\infty}^{t}\frac{\phi(t')-\phi(t)}{[2\pi i(t-t')/\mu]^{3/2}}dt' \quad \text{(S13)}$$

where, on the right-hand side we have neglected terms of order $\mu^2\eta r_0^2|\partial_t\phi(t)|$. They are smaller than the integral term by a factor $\sqrt{\mu r_0^2/\tau}$ where τ is the characteristic time scale of variations of ϕ. For completeness we also explicitly write Eq. (S9) projected on the s-wave channel

$$i\partial_t\phi(t) = \nu(t)\,\phi(t) - \eta\,\Psi(r_0,t). \quad \text{(S14)}$$

The function $\Psi(r_0,t)$ is eliminated from Eqs. (S13-S14) and after partial integration the resulting equation for the closed-channel amplitude reads

$$i\partial_t\phi(t) - [\nu(t) - \mu\,\eta^2/(2\pi r_0)]\phi(t) - \frac{\eta^2}{\sqrt{2i}}\left(\frac{\mu}{\pi}\right)^{3/2}\int_{-\infty}^{t}\frac{\partial_{t'}\phi(t')}{\sqrt{t-t'}}dt' = -\eta e^{-ik^2t/(2\mu)}. \quad \text{(S15)}$$

In the stationary case (time-independent ν) Eq. (S15) is solved by $\phi(t) = \phi_0 e^{-ik^2t/(2\mu)}$ with

$$\phi_0 = -\frac{\eta}{k^2/(2\mu) - [\nu - \mu\eta^2/(2\pi r_0)] + i\mu\eta^2 k/(2\pi)} \quad \text{(S16)}$$

and Eq. (S10) becomes

$$\Psi(\mathbf{y},t) = e^{i\mathbf{k}\cdot\mathbf{y}-ik^2t/(2\mu)} + \frac{\mu\eta\phi_0}{2\pi}\frac{e^{iky-ik^2t/(2\mu)}}{y} \quad \text{(S17)}$$

valid for $y \geq r_0$. In Eq. (S17) one recognizes the scattering amplitude $f(k) = \mu\eta\phi_0/(2\pi)$. Identifying

$$\eta = \sqrt{\frac{\pi}{\mu^2 R^\star}} \quad \text{(S18)}$$

and

$$E_0 = \nu - \frac{1}{2\mu R^\star r_0} \quad \text{(S19)}$$

we recover the standard narrow-resonance structure of the scattering amplitude

$$f(k) = -\frac{1}{R^\star(k^2 - 2\mu E_0) + ik} \quad \text{(S20)}$$

and the stationary closed-channel amplitude equals

$$\phi_0 = -\frac{2\sqrt{\pi/R^\star}}{k^2 - 2\mu E_0 + ik/R^\star}. \quad \text{(S21)}$$

Substituting Eqs. (S18-S19) into Eq. (S15) we obtain the evolution equation with renormalized parameters

$$i\partial_t\phi(t) - E_0(t)\,\phi(t) - \frac{1}{\sqrt{2\pi i\mu}\,R^\star}\int_{-\infty}^{t}\frac{\partial_{t'}\phi(t')}{\sqrt{t-t'}}dt' = -\sqrt{\frac{\pi}{\mu^2 R^\star}}\,e^{-ik^2t/(2\mu)}. \quad \text{(S22)}$$

To reproduce Eq. (4) of the main text we should set $\mu = m/2$ and multiply the right-hand side of Eq. (S22) by $\sqrt{2}$, which takes into account the correct symmetrization of the incoming wave for identical bosons $\Psi_0(\mathbf{y},t) = \sqrt{2}\cos(\mathbf{k}\cdot\mathbf{y})e^{-ik^2t/(2\mu)}$. Accordingly, the stationary contact density of a thermal Bose gas reported in Eq. (5) of the main text is obtained from Eq. (S21) multiplied by $\sqrt{2}$ and where we set $\mu = m/2$.

We emphasize that our theory is valid in the zeroth order in the small parameter $\sqrt{\mu r_0^2/\tau}$ [see discussion after Eq. (S13)]. For the stationary case the characteristic time of variation of ϕ

is $\tau \sim \mu/k^2$ and the small parameter becomes $r_0 k$. In practice this means that we cannot go beyond ultracold temperatures and describe quenches on timescales associated with the interaction range.

As we explain in the main text, the knowledge of ϕ for a pair of atoms in a unit volume can be used for determining the contact density. This statement is based on the observation, which holds also in the nonstationary case under the condition $\sqrt{\mu r_0/\tau} \ll 1$, that the closed-channel amplitude $\phi(t)$ is related to the $1/y$ singularity of $\Psi(y,t)$ by $\phi(t) = \sqrt{4\pi R^\star}\lim_{y\to 0} y\,\Psi(y,t)$. In the stationary case this follows directly from Eq. (S17); in the general case it can be seen by keeping in Eq. (S13) only terms diverging as $1/r_0$. Namely, we have $\Psi(r_0,t) = \mu\eta\phi(t)/(2\pi r_0)$, which, by using Eq. (S18), reduces to $\phi(t) = \sqrt{4\pi R^\star}\, r_0\, \Psi(r_0,t)$.

Finally we note that in the broad-resonance limit ($R^\star \to 0$), the $\dot\phi$ term drops out in Eq. (4) of the main text, which implies that the function $\phi(t)/\sqrt{R^\star} \propto \lim_{r\to 0} r\,\Psi(\mathbf{r},t)$ solves the integral equation already obtained in Ref. [10].

Single-quench evolution of $\mathcal{C}_2(t)$

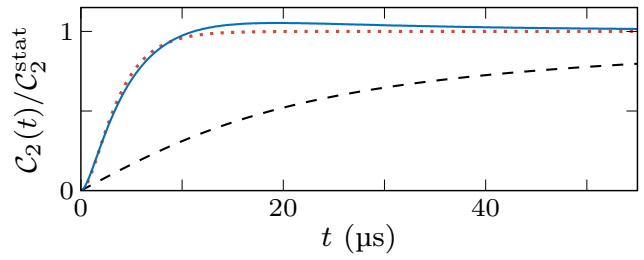

FIG. S6. Single-quench evolution of $\mathcal{C}_2(t)$. Evolution of $\mathcal{C}_2(t)$, scaled by its stationary value, for $T = 0.4\,\mu$K. Blue line: numerical computation for $R^\star = 10\ell_{\rm vdW}$ and $\Gamma_{\rm b}/2\pi = 123\,$kHz. Red dotted line: asymptotic expression in the lossy narrow resonance limit, see main text, for $\Gamma_{\rm b}/2\pi = 123\,$kHz. Black dashed line: asymptotic expression in the lossless broad resonance limit, see main text.

Based on Eq. (6) of the main text, we take the inverse Laplace transform of $\phi(s)$ and numerically compute the thermal average of $|\phi(t)|^2$, which allows us to extract the single-quench evolution of $\mathcal{C}_2$ for our experimental parameters $R^\star = 10\ell_{\rm vdW}$ and $\Gamma_{\rm b}/2\pi = 123\,$kHz (see Eq. (7) of main text). In Fig. S6, we compare the numerical results, for $T = 0.4\,\mu$K, to the asymptotic formulas obtained in the lossless broad limit, $\mathcal{C}_2(t)/\mathcal{C}_2^{\rm stat} = 2\arctan(t/\tau_T)/\pi$, and lossy narrow resonance limit, $\mathcal{C}_2(t)/\mathcal{C}_2^{\rm stat} = (1-e^{-\Gamma_{\rm b}t/2})^2$. We note that for narrow resonances, $\mathcal{C}_2(t)$ can become non-monotonic, whereas for broad resonances this only occurs when quenching to the $\mathrm{Re}(E_0) < 0$ side of the resonance [4].

Floquet analysis

For time-periodic $E_0(t)$ with period $2\pi/\Omega$ we use the formalism of Ref. [2] and solve the integro-differential Eq. (S22) by decomposing $\phi(t)$ in the Floquet channels

$$\phi(t) = \sum_{n=-\infty}^{\infty} \phi_n e^{-i\omega_n t}, \tag{S23}$$

where $\omega_n = \Omega n + k^2/(2\mu)$. Substituting this expansion into Eq. (S22) and using the equality

$$\int_{-\infty}^{t} \frac{e^{-i\omega t'} - e^{-i\omega t}}{(t-t')^{3/2}} dt' = -e^{-i\omega t}\sqrt{2\pi|\omega|}(1 - i\,\mathrm{sign}\,\omega), \tag{S24}$$

valid for real ω, we obtain

$$\left[\frac{\pi}{2}\sqrt{\frac{|\omega_n|}{i\mu}}(1 - i\,\mathrm{sign}\,\omega_n) - \omega_n\right]\phi_n + \sum_{m=-\infty}^{\infty} D_{n-m}\phi_m = \sqrt{\frac{\pi}{\mu^2 R^*}}\delta_{n0}, \tag{S25}$$

where D_n is the Fourier transform

$$D_n = \frac{\Omega}{2\pi}\int_0^{2\pi/\Omega} e^{i\Omega n t} E_0(t) dt \tag{S26}$$

and δ_{nm} is the Kronecker delta. Denoting by $E_0^{\rm on}$ the value of the (complex) detuning at times $0 < t < t_{\rm on}$ and $E_0^{\rm off}$ at times $t_{\rm on} < t < t_{\rm on} + t_{\rm off}$ the Fourier transform of the infinite sequence of square pulses ($t_{\rm on} + t_{\rm off} = 2\pi/\Omega$) reads

$$D_{n=0} = \frac{\Omega}{2\pi}(E_0^{\rm on} t_{\rm on} + E_0^{\rm off} t_{\rm off}), \tag{S27}$$

$$D_{n\neq 0} = \frac{e^{i\Omega n t_{\rm on}} - 1}{2\pi i n}(E_0^{\rm on} - E_0^{\rm off}). \tag{S28}$$

We solve Eq. (S25) numerically by introducing a cutoff for sufficiently high $|n|$ ensuring convergence. The vector ϕ_n [or $\phi(t)$ given by Eq. (S23)] can then be used for calculating all relevant observables (the contact, the instantaneous or averaged loss rate, etc.)

* raphael.lopes@lkb.ens.fr

[1] B. S. Rem, A. T. Grier, I. Ferrier-Barbut, U. Eismann, T. Langen, N. Navon, L. Khaykovich, F. Werner, D. S. Petrov, F. Chevy, and C. Salomon, Lifetime of the Bose Gas with Resonant Interactions, Phys. Rev. Lett. **110**, 163202 (2013).

[2] A. G. Sykes, H. Landa, and D. S. Petrov, Two-and three-body problem with Floquet-driven zero-range interactions, Phys. Rev. A **95**, 062705 (2017).

[3] M. Sun, P. Zhang, and H. Zhai, High Temperature Virial Expansion to Universal Quench Dynamics, Phys. Rev. Lett. **125**, 110404 (2020).

[4] J.-N. Cui, Z. Zhou, and M. Sun, Universal dynamic scaling and Contact dynamics in quenched quantum gases, Frontiers of Physics **19**, 22201 (2024).
[5] X. Yang and R. Zhang, Quench dynamics of thermal Bose gases across wide and narrow Feshbach resonances, Phys. Rev. A **107**, 063310 (2023).
[6] L. Pricoupenko, Many Bosons in a Narrow Magnetic Feshbach Resonance, Phys. Rev. Lett. **110**, 180402 (2013).
[7] L. Zhou and X. Cui, Effective scattering and Efimov physics in the presence of two-body dissipation, Phys. Rev. Res. **3**, 043225 (2021).
[8] E. Braaten, D. Kang, and L. Platter, Universal relations for a strongly interacting Fermi gas near a Feshbach resonance, Phys. Rev. A **78**, 053606 (2008).
[9] A. Pricoupenko and D. S. Petrov, Three-body interaction near a narrow two-body zero crossing, Phys. Rev. A **100**, 042707 (2019).
[10] R. Qi, Z. Shi, and H. Zhai, Maximum energy growth rate in dilute quantum gases, Phys. Rev. Lett. **126**, 240401 (2021).